ACS APPLIED MATERIALS & INTERFACES

www.acsami.org

Research Article

Effects of Boron Doping on the Bulk and Surface Acoustic Phonons in Single-Crystal Diamond

Erick Guzman, Fariborz Kargar,* Frank Angeles, Reza Vatan Meidanshahi, Timothy Grotjohn, Aaron Hardy, Matthias Muehle, Richard B. Wilson, Stephen M. Goodnick, and Alexander A. Balandin*

Cite This: https://doi.org/10.1021/acsami.2c10879

Read Online

ACCESS | Metrics & More | Article Recommendations | Supporting Information

ABSTRACT: We report the results of the investigation of bulk and surface acoustic phonons in the undoped and boron-doped single-crystal diamond films using the Brillouin–Mandelstam light scattering spectroscopy. The evolution of the optical phonons in the same set of samples was monitored with Raman spectroscopy. It was found that the frequency and the group velocity of acoustic phonons decrease nonmonotonically with the increasing boron doping concentration, revealing pronounced phonon softening. The change in the velocity of the shear-horizontal and the high-frequency pseudo-longitudinal acoustic phonons in the degenerately doped diamond, as compared to that in the undoped diamond, was as large as ∼15% and ∼12%, respectively. As a result of boron doping, the velocity of the bulk longitudinal and transverse acoustic phonons decreased correspondingly. The frequency of the optical phonons was unaffected at low boron concentration but experienced a strong decrease at the high doping level. The density-functional-theory calculations of the phonon band structure for the pristine and highly doped samples confirm the phonon softening as a result of boron doping in diamond. The obtained results have important implications for thermal transport in heavily doped diamond, which is a promising material for ultra-wide-band-gap electronics.

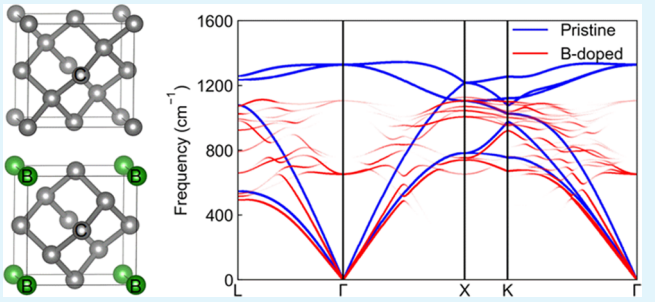

KEYWORDS: *ultra-wide-band-gap materials, diamond, Brillouin light scattering, Raman spectroscopy, phonon softening*

INTRODUCTION

Recent years witnessed a rapid growth of interest in ultra-wide band-gap (UWBG) semiconductors for applications in power electronics.[1−4] The materials, which belong to the UWBG group, include semiconductors such as AlN and diamond, with an electronic band gap ranging from 3 to 6 eV.[3] Among UWBGs, diamond attracts the most attention as it holds a record-high current density, thermal conductivity, mechanical stiffness, chemical stability, and the critical electric field.[5−9] Intrinsic diamond is an electrical insulator; it is doped by boron (B) to become a p-type semiconductor, suitable for electronic applications.[10] In diamond, the bulk acoustic phonons, i.e., quanta of crystal lattice vibrations, are the main heat carriers. They have high group velocities and long lifetimes.[7−9] These characteristics are responsible for diamond's high thermal conductivity of ∼2200 W m^{-1} K^{-1} at room temperature (RT) and excellent thermal interface conductance.[1,7−9,11] The frequency and dispersion of acoustic phonons are also related to the elastic and mechanical properties of the material. While boron substitutional doping improves the electrical conductivity of diamond, it adversely affects its phonon heat conduction characteristics.[12−14] Boron atoms act as point defects, scattering acoustic phonons, shortening their lifetime, and thus reducing the thermal conductivity of the material.[12−15] Although the phonons in diamond have been investigated extensively, the data on the surface and bulk acoustic phonons in the doped diamond are scarce and rather controversial. An important open question is "Do boron atoms only act as the scattering centers for acoustic phonons, which retain the frequency and velocity of intrinsic diamond, or do the dopant atoms alter the phonon characteristics of the material themselves?" The effect of doping on the surface acoustic phonons in diamond has also not been addressed. The properties of the surface phonons are important for understanding the thermal transport across interfaces in the device structures.

Brillouin–Mandelstam light scattering (BMS), also referred to as Brillouin light spectroscopy (BLS), is a nondestructive optical technique that has been used extensively to study acoustic phonons in different types of materials.[16] This technique has been employed to examine the mechanical

Received: June 18, 2022
Accepted: August 29, 2022

properties of different types of diamond, e.g., polycrystalline, smooth fine-grained, and single-crystal diamond grown by chemical vapor deposition (CVD) method.[17−20] The prior studies reported the characteristics of bulk longitudinal acoustic (LA) and transverse acoustic (TA) phonons as well as the traveling surface acoustic waves (SAWs) along the high-symmetry crystallographic directions.[19,20] The elasticity coefficients of diamond were extracted from BMS data.[17−20] A recent detailed study has used the angle-resolved BMS to find the properties of SAWs along different crystallographic directions in diamond.[21] No BMS data on the effect of boron on bulk and surface acoustic phonons in boron-doped diamond have been reported to date. In this work, we used the BMS technique to investigate the bulk and surface acoustic phonons in the low, medium, and highly boron-doped CVD-grown diamond films and compared the results to that of the undoped high-pressure high-temperature (HPHT) diamond. The evolution of optical phonons in the same samples was monitored with Raman spectroscopy. It was found that the frequency and group velocity of acoustic phonons decrease nonmonotonically with the increasing boron doping concentration, revealing pronounced phonon softening. The phonon modification with the introduction of dopant atoms appears to be stronger than previously believed. The observed changes in the characteristics of acoustic phonons in diamond because of doping have important broad implications for heat conduction in UWBG materials and for the thermal management of UWBG-based electronic devices.[22]

RESULTS OF MEASUREMENTS

The single-crystal diamond films for this study have been grown by the CVD method on the HPHT diamond substrate synthesized via the high-pressure high-temperature method. The details of the growth and boron doping procedures have been reported by some of us elsewhere.[23,24] The quality of the CVD diamond and characteristics of optical phonons were assessed with Raman spectroscopy. The samples with the boron doping concentrations of 10^{16}, 10^{17}, and 3×10^{20} cm^{-3} were referred to as the low-doped, medium-doped, and highly doped diamond, respectively. Systematic Raman measurements were conducted using a 633 nm wavelength excitation laser in a conventional backscattering configuration. The laser power was kept low at ∼60 μW all the time to eliminate any possible laser-induced heating effects. In Figure 1a, we present typical Raman spectra for all types of diamond films and the reference HPHT diamond. Comparing the data, one finds additional Raman features appearing as broad peaks in the range of 300−1300 cm^{-1} in the sample with the highest boron doping concentration. These broad bands at ∼550, 900, 1050, and 1200 cm^{-1} tend to appear in boron-doped diamond samples. Their intensity and spectral position can differ at concentrations close to the insulator-to-metal transition.[25] The transition occurs at high boron doping similar to our highly B-doped sample. These peaks are activated in diamond as a result of some structural disorder induced by high boron inclusion.[26,27] The broad bands near 1200 and 550 cm^{-1} are generally attributed to the forbidden Raman peaks that correspond to the maximum phonon density of states and the maximum density of states of the acoustic phonons in diamond, respectively.[28] More detailed discussions of these peaks are provided in refs 26, 28. In all spectra, the intense peak at ∼1332 cm^{-1} originates from the Brillouin zone (BZ)

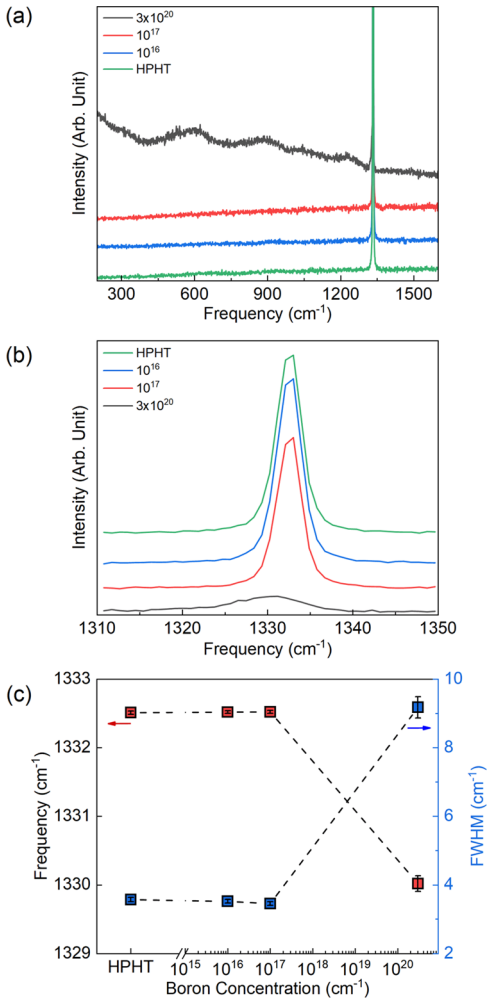

Figure 1. (a) Raman spectra of the boron-doped diamond samples and a reference undoped HPHT diamond recorded under a 633 nm excitation laser. (b) Raman spectra for the same samples in the vicinity of the diamond's zone-center optical phonon peak at ∼1332 cm^{-1}. (c) Spectral position (red squares) and full width at half-maximum (FWHM) (blue squares) of the zone-center peak as a function of the boron concentration. The spectral position of the peak decreases by 2 cm^{-1}, while its FWHM increases significantly for the highly doped diamond.

center optical phonons of diamond, referred to here as the zone-center phonons (ZCPs).[26,28]

Figure 1b shows the details of the ZCP Raman signatures. The intensity of the ZCP peak is lower in the highly doped diamond compared to that of other samples. The peak is symmetric for all types of samples, and we were able to fit the experimental data accurately using a single Lorentzian function. Several prior Raman studies have reported that boron doping induces an asymmetry in the ZCP peak, which changes its shape from a Lorentzian-like to a Fano-like peak.[26,28] The latter is explained by an increased contribution of scattering by free charge carriers in the highly doped samples.[28] We also observed such evolution of Raman spectra collected under 488 nm and 325 nm wavelength laser excitation (see the Supporting Information). Since no changes in the symmetry of the ZCP peak were seen in Raman spectra accumulated under the 633 nm laser excitation, we concluded that the behavior of the ZCP peak depends strongly on the wavelength of the excitation laser.

https://doi.org/10.1021/acsami.2c10879
ACS Appl. Mater. Interfaces XXXX, XXX, XXX−XXX

In Figure 1c, we show the spectral position and the full width at half-maximum (FWHM) of this Raman peak determined using the Lorentzian fittings. The exact data are also provided in the table format in the Supporting Information. The spectral position and the FWHM of the optical phonons remain unchanged for the low- and medium-boron-doped samples compared to those for the undoped HPHT reference sample. In the highly doped diamond, however, the ZCP peak red-shifts by ~2 cm^{-1}, exhibiting the optical phonon softening behavior. The change in the spectral position of the ZCP Raman peak is higher than the hardware resolution of our Raman system, which is ~1 cm^{-1}. Moreover, its FWHM, which inversely relates to the phonon lifetime,[29] increases by a factor of ~3 compared to the undoped HPHT and low and medium-doped samples. This is consistent with the observation that structural disorder can also make FWHM wider.[30] If the structural disorder has a length scale L, phonons with the wavelength $q \sim 1/L$ will contribute to the scattering and, as a result, broaden the energy spectrum and lower the average energy of the first-order Raman peak.[31] Possible implications of the optical phonon softening on thermal transport in diamond are discussed below.

We now turn to the main element of this work—BMS investigation of the boron-doped diamond films. The BMS measurements were conducted in the backscattering configuration using a 532 nm excitation laser at a fixed light incident angle $\theta = 20°$. The incident light was p-polarized; no specific polarization selection was used for the collection of the scattered light. The details of our BMS procedures are provided in the Methods section and prior reports for other material systems.[16,32,33] The top surfaces of the samples were the diamond's (001) crystallographic plane with an off-cut plane angle of ~3°. This small off-cut angle had a negligible effect on the light scattering and did not affect the interpretation of BMS data. Figure 2 shows the results of the BMS measurements of the three boron-doped diamond samples and the HPHT diamond substrate in the frequency range of 25−250 GHz. Two sharp peaks on each side of the spectra are associated with the Stokes and anti-Stokes scattering processes by the LA and TA bulk phonons. The spectral position of the observed peaks, f, was determined accurately by fitting the experimental with individual Lorentzian functions. The details of the fitting procedures are provided in the Supporting Information. The phonon wavevector of these bulk modes is, $q_B = 4\pi n/\lambda$, where λ is the wavelength of the excitation laser and n is the refractive index of the medium.[16,34] Table 1 summarizes the peak frequency, FWHM, and the relative intensity of LA to TA modes for all diamond samples.

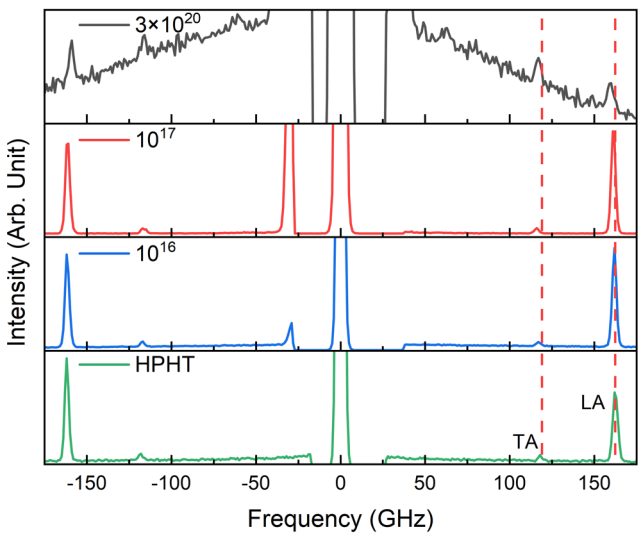

Figure 2. Brillouin light scattering spectra of the boron-doped diamond samples in the backscattering geometry performed at a 20° incidence angle. The dashed lines are guides to the eye to illustrate the decrease in the acoustic phonon frequency as the doping level increases. The peaks labeled as LA and TA correspond to the longitudinal acoustic and the transverse acoustic bulk phonons, respectively.

Table 1. Spectral Position, FWHM, and Relative Intensity of BMS Peaks in Three Diamond Samples

boron doping (cm^{-3})	f_{TA} (GHz)	$FWHM_{TA}$ (GHz)	f_{LA} (GHz)	$FWHM_{LA}$ (GHz)	I_{LA}/I_{TA}
HPHT	117.9	2.3	162.4	2.7	16.7
10^{16}	117.1	4.4	161.9	2.4	24.8
10^{17}	115.9	3.5	161.3	2.3	20.5
3×10^{20}	116.9	2.9	159.5	2.6	1.0

It follows from the data in Table 1 that the LA and TA phonon modes experience softening with an increase in the boron doping level. The LA phonons have a frequency of 162.4 GHz in the undoped HPHT sample. It decreases to 159.5 GHz in the diamond with the highest boron concentration. The frequency of the TA phonons decreases from 117.9 to 116.9 GHz as the boron concentration increases. The FWHM of the peaks does not reveal a clear trend. The latter could be attributed to large experimental uncertainty in determining FWHM. An intriguing observation is that the relative intensity of the LA phonon peak with respect to the TA phonon, I_{LA}/I_{TA}, decreases substantially for the highest-doped diamond. In optically isotropic materials and in the backscattering BMS configuration, the spectral power scattered by TA phonons falls to zero and therefore the spectrum is dominated by the LA peak.[34] In our results, this is the case for the low- and medium-doped diamond samples. However, in high-boron-doped diamond, the scattering intensity of the LA peaks is suppressed significantly, becoming even weaker than the associated TA peak. Given that the I_{LA}/I_{TA} ratio in the BMS strongly depends on the boron concentration, one can use this parameter to determine the local boron doping with a spatial resolution of 25 μm and 1 μm using the regular- and micro-BMS systems, respectively.

Knowing the frequency of the phonon modes, f, and the probed phonon wavevector, q_B, one can also obtain the phase velocity, v_p, of the phonons as $v_p = 2\pi f/q_B$. Note that since the dispersion of acoustic phonons close to the Brillouin zone center is linear, i.e., $\omega = qv_p$, the phase velocity, $vp = \omega q$, and the group velocity, $v_g = \partial\omega/\partial q$, of the fundamental LA and TA acoustic phonons are essentially the same, i.e., $v_p = v_g$. In our experiments, the direction of the examined phonon wavevector lies close to the [001] real-space crystallographic direction with a deviation angle of θ^* from the [001] direction. The deviation angle can be calculated using Snell's law, as $\sin(\theta^*) = \sin(\theta)/n$, in which n is the diamond's index of refraction and $\theta = 20°$ is the incident angle fixed for all measurements. The characteristics of acoustic phonons depend on the crystallographic direction, and thus possible changes due to θ^* should be

https://doi.org/10.1021/acsami.2c10879
ACS Appl. Mater. Interfaces XXXX, XXX, XXX−XXX

considered. We measured the change in the refractive index of the boron-doped diamond samples due to the boron dopants to account for this effect (see the Methods section). For the low- and medium-doped samples, the refractive index, measured at a 515 nm wavelength, was 2.43, whereas for the highest-doped sample, it reduced slightly to 2.41. The measured values of n and the respective deviation angle and the calculated group velocity of TA and LA phonons are summarized in Table 2. The calculated values for the reference

Table 2. Index of Refraction and Group Velocity of Fundamental Phonon Modes

boron doping (cm^{-3})	n at 515 nm	θ^a (degrees)	$v_{g,TA}$ (ms^{-1})	$v_{g,LA}$ (ms^{-1})
HPHT	2.3812[a]	8.26	13170.42	18141.44
10^{16}	2.43	8.09	12844.56	17713.95
10^{17}	2.43	8.09	12678.35	17650.52
3×10^{20}	2.41	8.17	12683.75	17651.62

[a]Ref 35.

HPHT sample are in good agreement with the reported data in the literature.[18,21] Note that the calculated values of v_g may inherit some error due to the measurement of n at a wavelength slightly different from that used in BMS experiments. We expect a similar variation in n at the laser excitation wavelength used in BMS. From these data, one can see that the group velocity of TA and LA phonons decreases with the boron incorporation. To further support our conclusions and reduce the uncertainty due to measurements of n, θ^* and Lorentzian fitting, which are always present in experiments with bulk phonons, we examined closely the characteristics of the surface acoustic phonons in the undoped and doped diamond samples.

In BMS experiments, light can also be scattered by the propagating surface ripples caused by the displacement fields of surface phonons or reflected bulk phonons from the interfaces.[16,34,36] In this scattering mechanism, the phonon wavevector, defined as $q_{||} = 4\pi \sin(\theta)/\lambda$, lies parallel to the surface of the sample. This wavevector only depends on the light incident angle, θ, and the wavelength of the excitation laser in vacuum, λ. The change in the incidence angle, θ, changes the frequency of the surface phonons owing to the variation in the phonon wavevector; the frequency of the bulk phonons remains almost constant. It is important to note that in the case of the surface phonons, the probing phonon wavevector is no longer a function of the refractive index, n. For this reason, all of the uncertainties, associated with the calculation of the velocities for bulk phonons and deviation angles from the high-symmetry [001] crystallographic direction, are eliminated. Figure 3 presents the results of the surface Brillouin scattering measurements performed at a constant incident angle of $\theta = 75°$. The calculated in-plane phonon wavevector is $q_{||} = 0.0228$ nm^{-1}. Two pronounced peaks are attributed to the shear-horizontal surface wave (SHW) and high-frequency pseudo-longitudinal wave (HFPLW).[17,21] The important observation is that the frequencies of these peaks decrease with an increasing boron doping concentration in diamond. The latter provides solid evidence for the phonon softening in the acoustic polarization branches.

The frequency, f, and the phase velocity of the SAW phonons, $v_p = 2\pi f/q_{||}$, are presented as the functions of the

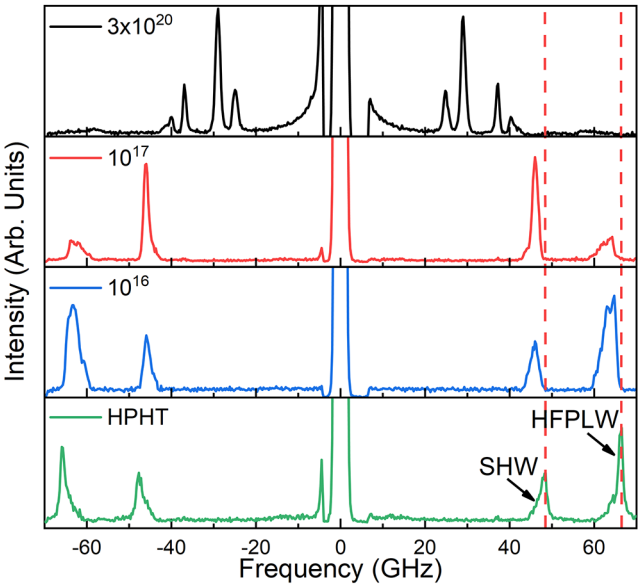

Figure 3. Brillouin light scattering spectra of the boron-doped diamond samples and a reference HPHT diamond substrate accumulated at $\theta = 75°$. The shear-horizontal surface wave and high-frequency pseudo-longitudinal wave are labeled as SHW and HFPLW, respectively. The frequency of types of phonons decreases as the boron concentration increases.

boron concentration in Figure 4. One can see that doping the diamond with boron at a low concentration of 10^{16} cm^{-3}

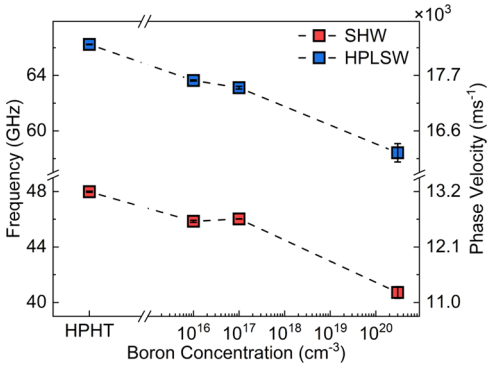

Figure 4. Frequency and velocity of surface phonons in diamond as a function of the boron doping concentration. The data for the SHW and HPLSW phonon polarization branches are shown at $q_{||} = 0.0228$ nm^{-1}.

makes the phase velocity of both phonon branches to decrease as compared to that of the undoped reference HPHT diamond. Additional doping of the diamond sample up to 10^{17} cm^{-3} does not strongly affect the phonon velocity. However, for the heavily doped diamond, with a boron concentration of 3×10^{20} cm^{-3}, another strong decrease in the phase velocity is observed. This nonmonotonic trend is similar to what has been reported previously by some of us for the phonon softening in the doped alumina samples.[37] In the alumina, the low mass and small radius aluminum (Al) atoms were substituted with the heavy and large radius neodymium (Nd) atoms.[37] In the boron-doped diamond, the situation is different. On the atomic scale, boron is slightly lighter than carbon, i.e., $m_B/m_C \sim 0.91$, and therefore, the variation in mass cannot explain the observed phonon softening. However,

https://doi.org/10.1021/acsami.2c10879
ACS Appl. Mater. Interfaces XXXX, XXX, XXX−XXX

boron's radius is slightly bigger than that of carbon, $R_B/R_C \sim 1.3$. Therefore, a possible mechanism for the phonon softening is the lattice distortion induced by the boron atoms. This distortion, especially in the heavily doped sample, causes an increase in the "effective" crystal lattice parameter and the atomic plane separation. This agrees well with the red shift observed in the Raman ZCP peak of diamond (see Figure 1b). An independent study confirms that the lattice constant of diamond slightly increases with the boron dopant concentration and starts to vary at a higher rate as the concentration surpasses $\sim 2.7 \times 10^{20}$ cm^{-3}.[38] Comparing the phonon phase velocity of the highly doped sample with that of the undoped HPHT diamond, one can see that the phonon velocity of the SHW and HFPLW polarization branches decreases by more than ~15 and ~11.7%, respectively.

In diamond, the phase velocity of the HFPLW is negligibly smaller than that of the bulk LA phonons traveling in the <001> direction.[18] The observed reduction in v_p of the HFPLW with the boron doping concentration points out that the phase velocity and correspondingly the group velocity of the respective LA phonon polarization branch experience similar softening. Such a reduction has important implications for the thermal and mechanical properties of boron-doped diamond. The phase velocity of SHW and HFPLW in diamond can be estimated from the equations $v_{SHW} = (c_{66/\rho})^{1/2}$ and $v_{HFPLW} = (c_{11/\rho})^{1/2}$, respectively, where ρ is the mass density.[18] Note that the phase velocities of SHW and HFPLW phonons depend only on one elasticity constant. Therefore, we can directly relate the elasticity parameters c_{66} and c_{11} to the measured phase velocities of these surface acoustic waves. Assuming a constant mass density for the boron-doped diamond samples, one can infer that the elastic constants decrease with boron addition, in line with the previously reported values obtained by other techniques.[39,40]

RESULTS OF MODELING

We performed phonon band structure calculations using the density functional theory (DFT) implemented in the Quantum Espresso 7.0 package[41] to investigate the effect of B-doping on the phonon energy dispersion in diamond. The details of the calculations can be found in the Methods section. We used a cube supercell containing eight atoms in the DFT calculations. For B-doped diamond, one of the C atoms was replaced by B, equivalent to the $\sim 2 \times 10^{22}$ cm^{-3} doping concentration. The structure of the supercells for the pristine and B-doped diamond is provided in the Supporting Information. To validate our modeling approach, the phonon dispersion of pure diamond was calculated using an FCC unit cell containing two carbon atoms with an experimental lattice constant of 3.57 Å. The computational results were compared with the experimental data from ref 42. The data presented in the Supporting Information indicate an excellent agreement between the calculated and experimental phonon frequencies.

After relaxation, the optimized lattice constants were obtained to be 3.54 and 3.60 Å for pristine and B-doped diamond supercells, respectively. The obtained lattice constant of pristine diamond agrees well with the measured lattice constant of 3.57 Å.[38] Figure 5a shows the calculated phonon dispersion of pristine diamond in comparison with that of the B-doped diamond with a boron concentration of $\sim 2 \times 10^{22}$ cm^{-3}. Since we used the supercell and thus smaller Brillouin zone, all phonon bands are folded back in the reciprocal space. To make the phonon dispersion easier to understand, we

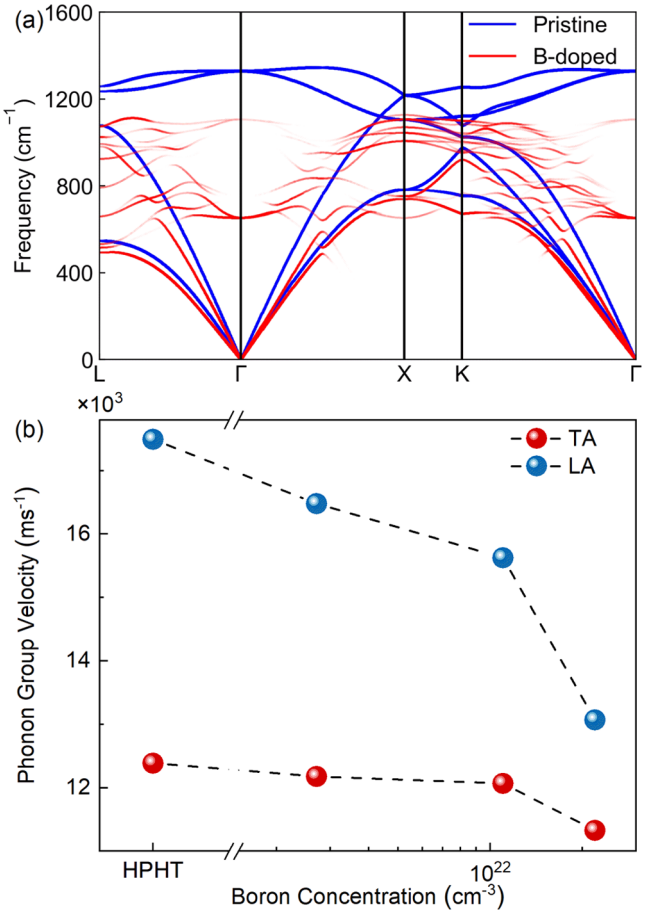

Figure 5. (a) Calculated phonon band structure of the pristine (blue) and B-doped (red) diamond. (b) The phonon group velocity of TA and LA modes close to the BZ center for pristine and B-doped diamond as a function of the boron concentration. The softening of all acoustic phonon modes as a result of boron doping is clearly observed. Note that we assumed a substantially higher concentration of B atoms to keep the supercell reasonably small in the calculations.

unfolded the supercell dispersion using the phonon unfolding package.[43] As a result, the phonon dispersion of pristine diamond is completely reproduced and the excess phonon modes at high-symmetry points for both pristine and B-doped diamond have been almost completely removed. As seen in Figure 5a, both the LA and TA phonon modes undergo softening as a result of the doping. We calculated the group velocity of LA and TA phonons near the BZ center for the pristine diamond and several values of boron concentrations. Note that we intentionally assumed higher boron concentrations in the simulations to keep the size of the supercell and the cost of calculations reasonable. The results are presented in Figure 5b. The calculated phonon velocities in pristine diamond for LA and TA modes along the Γ−X direction and close to the BZ center are 17,494 and 12,388 ms^{-1}, respectively. The obtained values agree well with our experimental measurements for the undoped HPHT diamond. In the B-doped diamond, the velocity for the LA and TA phonons decreases substantially. The change in the group velocity of the LA polarization branch is more pronounced compared to that of the TA mode, which is in qualitative agreement with our experimental observation. Note that since we considered 2-orders-of-magnitude higher boron concen-

https://doi.org/10.1021/acsami.2c10879
ACS Appl. Mater. Interfaces XXXX, XXX, XXX−XXX

tration in our simulations, we do not make a direct quantitative comparison of the velocities.

DISCUSSION

The phonon softening has interesting and important implications for thermal transport and related properties. Conventional theories of the thermal conductivity of semiconductor and insulating materials assume that doping does not modify the group velocity, v_g, of the acoustic phonons.[44−46] The dopants act as an extra point defect scattering centers for the acoustic phonons, which retain their properties the same as in the intrinsic material. However, if the phonon group velocity changes as a result of the doping, one needs to take it into account in the calculations.[47] In the kinetic theory, the phonon thermal conductivity can be expressed as $K = (1/3)\, C v_g\, \Lambda = (1/3) C v_g^2 \tau$, where C is the volumetric heat capacity, v_g is the average phonon group velocity, Λ is the phonon "gray" mean-free path, and τ is the combined phonon relaxation time, i.e., lifetime. The phonon relaxation time is defined by the scattering rate in different types of processes; it can be expressed as $\tau^{-1} = \tau_U^{-1} + \tau_d^{-1} + \tau_{e\text{-}ph}^{-1}$. Here, τ_U^{-1}, τ_d^{-1}, and $\tau_{e\text{-}ph}^{-1}$ are the phonon−phonon Umklapp scattering rate due to the crystal anharmonicity, phonon−defect scattering rate, and the electron−phonon scattering rate, respectively. The scattering rates are the function of both phonon frequency, ω, and phonon group velocity, v_g. The phonon−defect scattering, which includes scattering on dopant atoms, is the dominant mechanism at low temperatures.[48] Given the high Debye temperature of diamond ($\theta_D \sim 1870$ K), the phonon−defect scattering makes a significant contribution even at room temperature (RT). The phonon softening alters the thermal conductivity, K, not only via the combined relaxation time, τ, but also via the volumetric heat capacity, C, which is proportional to v_g^{-3}. The dependence on the phonon group velocity is due to the phonon density of states. The previously reported data on the heat capacity of boron-doped single-crystal HPHT diamond support our arguments.[49] In this study, the doped diamond samples with higher boron concentration revealed higher heat capacity. The authors have interpreted their observation as a possible inclusion of metallic particles during the growth process and thus the dominance of electron heat capacity at low temperatures.[49] However, their data can also be explained by the lower phonon group velocity. One should remember that in the bulk crystals the phonon group velocity is the same as the phonon phase velocity, and the observed reduction in the phonon velocity is equivalent for both.

The strongest effect from the phonon softening on thermal conductivity near RT is expected via the changes in the phonon−defect scattering rate. The average phonon group velocity for all three acoustic polarization branches is given by the expression[50]

$$v_g = 3\{(1/v_{T,1}) + (1/v_{T,2}) + (1/v_L)\}^{-1} \quad (1)$$

Here, $v_{T,1}$ and $v_{T,2}$ are the phonon group velocities for two TA phonon polarization branches, and v_L is the LA phonon group velocity. Given that in diamond transverse acoustic phonons along the <001> direction are degenerate, our experimental data show that all velocities that enter eq 1 experience a reduction in their values. The phonon scattering rate on point defects, like dopant atoms, is given as[51,52]

$$\tau_P^{-1} = (V_0 \Gamma \omega^4 / 4\pi v_g^3) \quad (2)$$

Here, V_0 is the volume per atom, and Γ is the scattering parameter, which depends linearly on the defect concentration. Γ is a measure of the point defect scattering strength.[53,54] If the properties of phonons had not changed, the increase in this scattering rate would be only due to the increase in the concentration of dopant atoms. As a result of the reduction in the phonon velocity, v_g, the effect of the doping becomes stronger and likely dependent on the crystallographic direction.

It is also illustrative to consider the effect of the acoustic phonon softening for dislocation scattering. At a high density of doping, the dopant atoms may form clusters of atoms that act similar to dislocation lines. The phonon scattering rate on dislocation lines is given as[50,55]

$$\tau_E^{-1} = (2^{1.5}/3^{3.5}) \eta N_D^E b_E^2 \gamma^2 \omega \{(1/2) + (1/24) [(1 - 2\nu)/(1 - \nu)]^2 [1 + \sqrt{2}\,(v_L/v_T)^2]^2\} \quad (3)$$

Here, N_D^E and b_E are the density and magnitude of Burgers vectors for the edge dislocations, respectively, η accounts for the orientation of the dislocation lines with respect to the direction of temperature gradient. γ and ν are the Grüneisen anharmonicity parameter and Poisson ratio, respectively. One can see from eq 3 that even a relative reduction in the phonon velocity for the LA and TA phonons can play a role since the scattering rate depends on $\sim(v_L/v_T)$.[4] The discussed dependencies result in intricate effects of phonon softening on heat conduction in diamond. They can lead to a stronger reduction in the thermal conductivity than the predictions of simple theory that does not account for the changes in the phonon velocity or more pronounced anisotropy in thermal conductivity if the dopant atoms have some preferential arrangements.

The effects of phonon softening on thermal conductivity are not limited to acoustic phonons alone. Indeed, the contribution of the optical phonons to the phonon thermal conductivity of diamond is negligible owing to their high frequency and small group velocity.[56,57] However, optical phonons provide scattering channels for the acoustic phonon branches.[9] The broadening of the ZCP peak in the highly doped diamond sample indicates a shortened phonon lifetime due to the increased contribution of boron atoms to the phonon scattering processes via point defects and electron−phonon processes. One can estimate the decay rate of the longitudinal optical (LO) phonons at the Brillouin zone center ($q = 0$) using Klemens' formula $\tau^{-1} \sim \delta\omega$, where τ is the phonon lifetime and $\delta\omega$ is the FWHM of the Raman ZCP peak.[57,58] The estimated values of τ for the undoped HPHT and the low- and medium-doped diamond samples are ∼11 ps, which is close to the measured lifetime of phonons in single-crystal diamond using other techniques.[59] Our data show that this value decreases to ∼3.7 ps for the highly doped sample, significantly lower than that of the HPHT and other lightly doped diamond samples. This reduction can be correlated well with the measured reduction in thermal conductivity.

CONCLUSIONS

We investigated the bulk and surface acoustic phonons in the boron-doped single-crystal diamond films using the Brillouin−Mandelstam light scattering spectroscopy. It was found that the frequency and the group velocity of acoustic phonons decrease nonmonotonically with the increasing boron doping

https://doi.org/10.1021/acsami.2c10879
ACS Appl. Mater. Interfaces XXXX, XXX, XXX−XXX

concentration, revealing pronounced phonon softening. As a result of boron doping, the velocity of the bulk longitudinal and transverse acoustic phonons decreased correspondingly. The frequency of the optical phonons was unaffected at low boron concentration but experienced a strong decrease at the high doping level. We also performed density functional theory to calculate the phonon band structure for the pristine and highly doped diamond. The theoretical results qualitatively confirm the phonon softening in both optical and acoustic polarization branches. The strong softening of the acoustic phonons—the main heat carriers in diamond—has important implications for thermal transport in such materials. Our results also demonstrate that the intensity ratio of the LA and TA phonons can be used to monitor the boron concentration in diamond.

METHODS

Boron-Doped Diamond Growth. The boron-doped diamond was grown by microwave plasma-assisted chemical vapor deposition using hydrogen and methane feed gases, with the boron added during the homoepitaxial growth using diborane feed gas. The substrates used were HPHT seeds that were prepared with an off-cut angle of the growth surface of ∼3° from the (001) crystal plane. The boron concentrations were estimated based on similarly grown samples grown with equivalent conditions that were measured by secondary ion mass spectroscopy (SIMS) at EAG.

Brillouin–Mandelstam Spectroscopy. BMS experiments were conducted in the conventional backscattering configuration using a 532 nm laser excitation wavelength at several different incident angles. The light source was a solid-state diode-pumped continuous-wave laser (Spectra Physics). The laser beam was focused on the sample using a lens with NA=0.34. The scattered light was collected via the same lens and directed to the high-contrast high-resolution 3 + 3 pass tandem Fabry–Perot interferometer (TFP-1, JRS Optical Instruments, Switzerland) and spectrometer. For bulk and surface acoustic phonon measurements, the mirror spacing of the TFP interferometer was adjusted to 0.5 and 2 mm, respectively.

Refractive Index Measurements. The refractive index of the diamond thin films was determined by measuring the Fresnel reflectance coefficients for s- and p-polarized 515 nm lights. For the reflectance measurements, we use a linearly polarized laser beam with a polarization of 45° from the vertical. We focused the light on the sample using a 10× objective lens. The angle of incidence of the beam with the sample was kept at 45°. Light reflected from the sample was collected by another 10× objective lens. The light that reflected from the sample's back surface was spatially separated from the primary reflected beam with an aperture. The intensity and polarization of the reflected probe beam were measured by a calibrated power meter and a polarimeter. We used a multilayer optical calculation to analyze the reflectance data. The index of refraction of the diamond film was treated as a fitting parameter until the model predictions matched the experimental observations for the polarization and intensity of the reflected laser beam.

Density-Functional-Theory (DFT) Calculations. The ultra-soft pseudopotential and the generalized gradient approximation (GGA) of the Perdew–Burke–Ernzerhof (PBE)[60] functional were employed to describe the core–valence electron interaction and exchange–correlation energy, respectively. The kinetic energy cutoff of 25 Ry was chosen for plane-wave basis sets. We use a cube supercell containing eight atoms in our DFT calculations. For boron-doped diamond, one of the C atoms was replaced by B, which was equivalent to the $\sim 2 \times 10^{22}$ cm^{-3} doping concentration. Both supercell size and atomic positions were relaxed using the BFGS quasi-Newton algorithm within DFT until the force on each atom was smaller than 0.001 Ry/Bohr. In the self-consistent ground-state calculations, an 8 × 8 × 8 Monkhorst–Pack *k*-point setting was used in the reciprocal space integration. After obtaining the self-consistent ground state, we performed the density functional perturbation theory (DFPT)[61] calculations with a uniform 4 × 4 × 4 grid of *q*-point setting. Then, we performed dynamical matrix Fourier transformations to obtain force constants and calculated the phonon dispersions. To benchmark our method of calculations, the phonon dispersion of pure diamond was calculated using an FCC unit cell containing two carbon atoms with an experimental lattice constant of 3.57 Å (Figure SX) and was compared with experimental data.[42]

ASSOCIATED CONTENT

Supporting Information

The Supporting Information is available free of charge at https://pubs.acs.org/doi/10.1021/acsami.2c10879.

Detailed description of the Raman and BMS measurements and simulations (PDF)

AUTHOR INFORMATION

Corresponding Authors

Fariborz Kargar − *Nano-Device Laboratory and Phonon Optimized Engineered Materials Center, Department of Electrical and Computer Engineering, University of California, Riverside, California 92521, United States;* orcid.org/0000-0003-2192-2023; Email: fkargar@ece.ucr.edu

Alexander A. Balandin − *Nano-Device Laboratory and Phonon Optimized Engineered Materials Center, Department of Electrical and Computer Engineering, University of California, Riverside, California 92521, United States;* orcid.org/0000-0002-9944-7894; Email: balandin@ece.ucr.edu

Authors

Erick Guzman − *Nano-Device Laboratory and Phonon Optimized Engineered Materials Center, Department of Electrical and Computer Engineering, University of California, Riverside, California 92521, United States*

Frank Angeles − *Department of Mechanical Engineering and Materials Science and Engineering Program, University of California, Riverside, California 92521, United States*

Reza Vatan Meidanshahi − *School of Electrical, Computer and Energy Engineering, Arizona State University, Tempe, Arizona 85281, United States*

Timothy Grotjohn − *Department of Electrical and Computer Engineering, Michigan State University, East Lansing, Michigan 48824, United States*

Aaron Hardy − *Fraunhofer USA Center Midwest, East Lansing, Michigan 48824, United States*

Matthias Muehle − *Fraunhofer USA Center Midwest, East Lansing, Michigan 48824, United States*

Richard B. Wilson − *Department of Mechanical Engineering and Materials Science and Engineering Program, University of California, Riverside, California 92521, United States*

Stephen M. Goodnick − *School of Electrical, Computer and Energy Engineering, Arizona State University, Tempe, Arizona 85281, United States;* orcid.org/0000-0002-2026-6274

Complete contact information is available at: https://pubs.acs.org/10.1021/acsami.2c10879

Author Contributions

A.A.B. and F.K. conceived the idea, coordinated the project, contributed to experimental data analysis, and led the manuscript preparation; E.G. conducted Raman and BMS experiments and contributed to the data analysis; F.K.

https://doi.org/10.1021/acsami.2c10879
ACS Appl. Mater. Interfaces XXXX, XXX, XXX−XXX

supervised the BMS experiments; F.A. conducted the refractive index measurements; T.G., A.H., and M.M. synthesized the B-doped diamond samples; R.W. supervised the refractive index measurements and assisted with the data analyses; R.V.M. conducted numerical simulations; and S.M.G. provided the theoretical calculations and assisted with data analysis. All authors contributed to the manuscript preparation.

Notes

The authors declare no competing financial interest.

■ ACKNOWLEDGMENTS

The work at UCR, ASU, and MSU was supported by ULTRA, an Energy Frontier Research Center (EFRC) funded by the U.S. Department of Energy, Office of Science, Basic Energy Sciences under Award # DE-SC0021230. A.A.B. and F.K. acknowledge the support of the National Science Foundation (NSF) for building a new type of Brillouin spectrometer provided via a Major Research Instrumentation (MRI) project DMR 2019056 entitled "Development of a Cryogenic Integrated Micro-Raman-Brillouin−Mandelstam Spectrometer". The authors thank Prof. Robert Nemanich, ASU, for useful discussions.

■ REFERENCES

(1) Malakoutian, M.; Field, D. E.; Hines, N. J.; Pasayat, S.; Graham, S.; Kuball, M.; Chowdhury, S. Record-Low Thermal Boundary Resistance between Diamond and GaN-on-SiC for Enabling Radio-frequency Device Cooling. *ACS Appl. Mater. Interfaces* **2021**, *13*, 60553−60560.

(2) Surdi, H.; Thornton, T.; Nemanich, R. J.; Goodnick, S. M. Space Charge Limited Corrections to the Power Figure of Merit for Diamond. *Appl. Phys. Lett.* **2022**, *120*, No. 223503.

(3) Ghosh, S.; Surdi, H.; Kargar, F.; Koeck, F. A.; Rumyantsev, S.; Goodnick, S.; Nemanich, R. J.; Balandin, A. A. Excess Noise in High-Current Diamond Diodes. *Appl. Phys. Lett.* **2022**, *120*, No. 062103.

(4) Tsao, J. Y.; Chowdhury, S.; Hollis, M. A.; Jena, D.; Johnson, N. M.; Jones, K. A.; Kaplar, R. J.; Rajan, S.; van de Walle, C. G.; Bellotti, E.; Chua, C. L.; Collazo, R.; Coltrin, M. E.; Cooper, J. A.; Evans, K. R.; Graham, S.; Grotjohn, T. A.; Heller, E. R.; Higashiwaki, M.; Islam, M. S.; Juodawlkis, P. W.; Khan, M. A.; Koehler, A. D.; Leach, J. H.; Mishra, U. K.; Nemanich, R. J.; Pilawa-Podgurski, R. C. N.; Shealy, J. B.; Sitar, Z.; Tadjer, M. J.; Witulski, A. F.; Wraback, M.; Simmons, J. A. Ultrawide-Bandgap Semiconductors: Research Opportunities and Challenges. *Adv. Electron. Mater.* **2018**, *4*, No. 1600501.

(5) Donato, N.; Rouger, N.; Pernot, J.; Longobardi, G.; Udrea, F. Diamond Power Devices: State of the Art, Modelling, Figures of Merit and Future Perspective. *J. Phys. D: Appl. Phys.* **2019**, *53*, No. 093001.

(6) Surdi, H.; Koeck, F. A. M.; Ahmad, M. F.; Thornton, T. J.; Nemanich, R. J.; Goodnick, S. M. Demonstration and Analysis of Ultrahigh Forward Current Density Diamond Diodes. *IEEE Trans. Electron Devices* **2022**, *69*, 254−261.

(7) Wei, L.; Kuo, P. K.; Thomas, R. L.; Anthony, T. R.; Banholzer, W. F. Thermal Conductivity of Isotopically Modified Single Crystal Diamond. *Phys. Rev. Lett.* **1993**, *70*, 3764−3767.

(8) Olson, J. R.; Pohl, R. O.; Vandersande, J. W.; Zoltan, A.; Anthony, T. R.; Banholzer, W. F. Thermal Conductivity of Diamond between 170 and 1200 K and the Isotope Effect. *Phys. Rev. B* **1993**, *47*, 14850−14856.

(9) Ward, A.; Broido, D. A.; Stewart, D. A.; Deinzer, G. Ab Initio Theory of the Lattice Thermal Conductivity in Diamond. *Phys. Rev. B* **2009**, *80*, No. 125203.

(10) Kalish, R. Doping of Diamond. *Carbon* **1999**, *37*, 781−785.

(11) Mandal, S.; Yuan, C.; Massabuau, F.; Pomeroy, J. W.; Cuenca, J.; Bland, H.; Thomas, E.; Wallis, D.; Batten, T.; Morgan, D.; Oliver, R.; Kuball, M.; Williams, O. A. Thick, Adherent Diamond Films on AlN with Low Thermal Barrier Resistance. *ACS Appl. Mater. Interfaces* **2019**, *11*, 40826−40834.

(12) Prikhodko, D.; Tarelkin, S.; Bormashov, V.; Golovanov, A.; Kuznetsov, M.; Teteruk, D.; Volkov, A.; Buga, S. Thermal Conductivity of Synthetic Boron-Doped Single-Crystal HPHT Diamond from 20 to 400 K. *MRS Commun.* **2016**, *6*, 71−76.

(13) Prikhodko, D.; Tarelkin, S.; Bormashov, V.; Golovanov, A.; Kuznetsov, M.; Teteruk, D.; Kornilov, N.; Volkov, A.; Buga, A. Low Temperature Thermal Conductivity of Heavily Boron-Doped Synthetic Diamond: Influence of Boron-Related Structure Defects. *J. Superhard Mater.* **2019**, *41*, 24−31.

(14) Williams, G.; Calvo, J. A.; Faili, F.; Dodson, J.; Obeloer, T.; Twitchen, D. J. In *Thermal Conductivity of Electrically Conductive Highly Boron Doped Diamond and Its Applications at High Frequencies*, Proceedings of the 17th InterSociety Conference on Thermal and Thermomechanical Phenomena in Electronic Systems; IEEE, 2018; pp 235−239.

(15) Ding, M.; Liu, Y.; Lu, X.; Li, Y.; Tang, W. Boron Doped Diamond Films: A Microwave Attenuation Material with High Thermal Conductivity. *Appl. Phys. Lett.* **2019**, *114*, No. 162901.

(16) Kargar, F.; Balandin, A. A. Advances in Brillouin−Mandelstam Light-Scattering Spectroscopy. *Nat. Photonics* **2021**, *15*, 720−731.

(17) Djemia, P.; Tallaire, A.; Achard, J.; Silva, F.; Gicquel, A. Elastic Properties of Single Crystal Diamond Made by CVD. *Diamond Relat. Mater.* **2007**, *16*, 962−965.

(18) Djemia, P.; Dugautier, C.; Chauveau, T.; Dogheche, E.; de Barros, M. I.; Vandenbulcke, L. Mechanical Properties of Diamond Films: A Comparative Study of Polycrystalline and Smooth Fine-Grained Diamonds by Brillouin Light Scattering. *J. Appl. Phys.* **2001**, *90*, 3771−3779.

(19) Grimsditch, M. H.; Ramdas, A. K. Brillouin Scattering in Diamond. *Phys. Rev. B* **1975**, *11*, 3139−3148.

(20) Jiang, X.; Harzer, J.; Hillebrands, B.; Wild, Ch.; Koidl, P. Brillouin Light Scattering on Chemical-Vapor-Deposited Polycrystalline Diamond: Evaluation of the Elastic Moduli. *Appl. Phys. Lett.* **1991**, *59*, 1055−1057.

(21) Xie, Y. R.; Ren, S. L.; Gao, Y. F.; Liu, X. L.; Tan, P. H.; Zhang, J. Measuring Bulk and Surface Acoustic Modes in Diamond by Angle-Resolved Brillouin Spectroscopy. *Sci. China: Phys., Mech. Astron.* **2021**, *64*, No. 287311.

(22) Turin, V. O.; Balandin, A. A. Electrothermal Simulation of the Self-Heating Effects in GaN-Based Field-Effect Transistors. *J. Appl. Phys.* **2006**, *100*, No. 054501.

(23) Ramamurti, R.; Becker, M.; Schuelke, T.; Grotjohn, T. A.; Reinhard, D. K.; Asmussen, J. Deposition of Thick Boron-Doped Homoepitaxial Single Crystal Diamond by Microwave Plasma Chemical Vapor Deposition. *Diamond Relat. Mater.* **2009**, *18*, 704−706.

(24) Demlow, S. N.; Rechenberg, R.; Grotjohn, T. The Effect of Substrate Temperature and Growth Rate on the Doping Efficiency of Single Crystal Boron Doped Diamond. *Diamond Relat. Mater.* **2014**, *49*, 19−24.

(25) Mortet, V.; Gregora, I.; Taylor, A.; Lambert, N.; Ashcheulov, P.; Gedeonova, Z.; Hubik, P. New Perspectives for Heavily Boron-Doped Diamond Raman Spectrum Analysis. *Carbon* **2020**, *168*, 319−327.

(26) Prawer, S.; Nemanich, R. J. Raman Spectroscopy of Diamond and Doped Diamond. *Philos. Trans. R. Soc., A* **2004**, *362*, 2537−2565.

(27) Ferrari, A. C.; Robertson, J. Resonant Raman Spectroscopy of Disordered, Amorphous, and Diamondlike Carbon. *Phys. Rev. B* **2001**, *64*, No. 075414.

(28) Mortet, V.; Živcová, Z. V.; Taylor, A.; Davydová, M.; Frank, O.; Hubík, P.; Lorincik, J.; Aleshin, M. Determination of Atomic Boron Concentration in Heavily Boron-Doped Diamond by Raman Spectroscopy. *Diamond Relat. Mater.* **2019**, *93*, 54−58.

(29) Menéndez, J.; Cardona, M. Temperature Dependence of the First-Order Raman Scattering by Phonons in Si, Ge, and -Sn: Anharmonic Effects. *Phys. Rev. B* **1984**, *29*, 2051−2059.

https://doi.org/10.1021/acsami.2c10879
ACS Appl. Mater. Interfaces XXXX, XXX, XXX−XXX

(30) Balkas, C.; Shin, H.; Davis, R.; Nemanich, R.; et al. Raman Analysis of Phonon Lifetimes in Aln and Gan of Wurtzite Structure. *Phys. Rev. B* **1999**, *59*, 12977−12982.
(31) Piscanec, S.; Cantoro, M.; Ferrari, A. C.; Zapien, J. A.; Lifshitz, Y.; Lee, S. T.; Hofmann, S.; Robertson, J. Raman Spectroscopy of Silicon Nanowires. *Phys. Rev. B* **2003**, *68*, 241312−242003.
(32) Kargar, F.; Debnath, B.; Kakko, J.-P.; Saÿnätjoki, A.; Lipsanen, H.; Nika, D. L.; Lake, R. K.; Balandin, A. A. Direct Observation of Confined Acoustic Phonon Polarization Branches in Free-Standing Semiconductor Nanowires. *Nat. Commun.* **2016**, *7*, No. 13400.
(33) Huang, C. Y. T.; Kargar, F.; Debnath, T.; Debnath, B.; Valentin, M. D.; Synowicki, R.; Schoeche, S.; Lake, R. K.; Balandin, A. A. Phononic and Photonic Properties of Shape-Engineered Silicon Nanoscale Pillar Arrays. *Nanotechnology* **2020**, *31*, No. 30LT01.
(34) Sandercock, J. R. Trends in Brillouin Scattering: Studies of Opaque Materials, Supported Films, and Central Modes. In *Light Scattering in Solids III. Topics in Applied Physics*; Cardona, M.; Güntherodt, G., Eds.; Springer: Berlin, Heidelberg, 1982; Vol. *51*; pp 173−206. DOI: 10.1007/3540115137_6.
(35) Zaitsev, A. M. *Optical Properties of Diamond*; Springer: Berlin, Heidelberg, 2001. DOI: 10.1007/978-3-662-04548-0.
(36) Mutti, P.; Bottani, C. E.; Ghislotti, G.; Beghi, M.; Briggs, G. A. D.; Sandercock, J. R. Surface Brillouin Scattering—Extending Surface Wave Measurements to 20 GHz. In *Advances in Acoustic Microscopy*; Briggs, A., Ed.; Springer: Boston, MA, 1995; Vol. *1*, pp 249−300.
(37) Kargar, F.; Penilla, E. H.; Aytan, E.; Lewis, J. S.; Garay, J. E.; Balandin, A. A. Acoustic Phonon Dispersion Engineering in Bulk Crystals via Incorporation of Dopant Atoms. *Appl. Phys. Lett.* **2018**, *112*, No. 191902.
(38) Brunet, F.; Germi, P.; Pernet, M.; Deneuville, A.; Gheeraert, E.; Laugier, F.; Burdin, M.; Rolland, G. The Effect of Boron Doping on the Lattice Parameter of Homoepitaxial Diamond Films. *Diamond Relat. Mater.* **1998**, *7*, 869−873.
(39) Liu, X.; Chang, Y. Y.; Tkachev, S. N.; Bina, C. R.; Jacobsen, S. D. Elastic and Mechanical Softening in Boron-Doped Diamond. *Sci. Rep.* **2017**, *7*, No. 42921.
(40) Wang, X.; Shen, X.; Sun, F.; Shen, B. Influence of Boron Doping Level on the Basic Mechanical Properties and Erosion Behavior of Boron-Doped Micro-Crystalline Diamond (BDMCD) Film. *Diamond Relat. Mater.* **2017**, *73*, 218−231.
(41) Giannozzi, P.; Baroni, S.; Bonini, N.; Calandra, M.; Car, R.; Cavazzoni, C.; Ceresoli, D.; Chiarotti, G. L.; Cococcioni, M.; Dabo, I.; Dal Corso, A.; de Gironcoli, S.; Fabris, S.; Fratesi, G.; Gebauer, R.; Gerstmann, U.; Gougoussis, C.; Kokalj, A.; Lazzeri, M.; Martin-Samos, L.; Marzari, N.; Mauri, F.; Mazzarello, R.; Paolini, S.; Pasquarello, A.; Paulatto, L.; Sbraccia, C.; Scandolo, S.; Sclauzero, G.; Seitsonen, A. P.; Smogunov, A.; Umari, P.; Wentzcovitch, R. M. QUANTUM ESPRESSO: A Modular and Open-Source Software Project for Quantum of Materials. *J. Phys.: Condens. Matter* **2009**, *21*, No. 395502.
(42) Warren, J. L.; Yarnell, J. L.; Dolling, G.; Cowley, R. A. Lattice Dynamics of Diamond. *Phys. Rev.* **1967**, *158*, 805−808.
(43) Zheng, F.; Zhang, P. Phonon Unfolding: A Program for Unfolding Phonon Dispersions of Materials. *Comput. Phys. Commun.* **2017**, *210*, 139−144.
(44) Klemens, P. G. Thermal Conductivity and Lattice Vibrational Modes. In *Solid State Physics*, Seitz, F.; Turnbull, D., Eds.; Academic Press, 1958; Vol. *7*, pp 1−98.
(45) Han, Y. J.; Klemens, P. G. Anharmonic Thermal Resistivity of Dielectric Crystals at Low Temperatures. *Phys. Rev. B* **1993**, *48*, 6033−6042.
(46) Callaway, J. Model for Lattice Thermal Conductivity at Low Temperatures. *Phys. Rev.* **1959**, *113*, No. 1046.
(47) Balandin, A.; Wang, K. L. Significant Decrease of the Lattice Thermal Conductivity Due to Phonon Confinement in a Free-Standing Semiconductor Quantum Well. *Phys. Rev. B* **1998**, *58*, No. 1544.
(48) Liu, W. L.; Shamsa, M.; Calizo, I.; Balandin, A. A.; Ralchenko, V.; Popovich, A.; Saveliev, A. Thermal Conduction in Nanocrystalline Diamond Films: Effects of the Grain Boundary Scattering and Nitrogen Doping. *Appl. Phys. Lett.* **2006**, *89*, No. 171915.
(49) Tarelkin, S.; Bormashov, V.; Kuznetsov, M.; Buga, S.; Terentiev, S.; Prikhodko, D.; Golovanov, A.; Blank, V. Heat Capacity of Bulk Boron-Doped Single-Crystal HPHT Diamonds in the Temperature Range from 2 to 400 K. *J. Superhard Mater.* **2016**, *38*, 412−416.
(50) Zou, J.; Kotchetkov, D.; Balandin, A. A.; Florescu, D. I.; Pollak, F. H. Thermal Conductivity of GaN Films: Effects of Impurities and Dislocations. *J. Appl. Phys.* **2002**, *92*, 2534−2539.
(51) Klemens, P. G. Heat Conduction in Solids by Phonons. *Thermochim. Acta* **1993**, *218*, 247−255.
(52) Liu, W.; Balandin, A. A. Thermal Conduction in AlxGa1-XN Alloys and Thin Films. *J. Appl. Phys.* **2005**, *97*, No. 073710.
(53) Herring, C. Role of Low-Energy Phonons in Thermal Conduction. *Phys. Rev.* **1954**, *95*, 954−965.
(54) Slack, G. A. Effect of Isotopes on Low-Temperature Thermal Conductivity. *Phys. Rev.* **1957**, *105*, 829−831.
(55) Kotchetkov, D.; Zou, J.; Balandin, A. A.; Florescu, D. I.; Pollak, F. H. Effect of Dislocations on Thermal Conductivity of GaN Layers. *Appl. Phys. Lett.* **2001**, *79*, 4316−4318.
(56) Sparavigna, A. Influence of Isotope Scattering on the Thermal Conductivity of Diamond. *Phys. Rev. B* **2002**, *65*, No. 064305.
(57) Liu, M. S.; Bursill, L. A.; Prawer, S.; Beserman, R. Temperature Dependence of the First-Order Raman Phonon Line of Diamond. *Phys. Rev. B* **2000**, *61*, 3391−3395.
(58) Solin, S. A.; Ramnas, A. K. Raman Spectrum of Diamond. *Phys. Rev. B* **1970**, *1*, 1687−1698.
(59) Lee, K. C.; Sussman, B. J.; Nunn, J.; Lorenz, V. O.; Reim, K.; Jaksch, D.; Walmsley, I. A.; Spizzirri, P.; Prawer, S. Comparing Phonon Dephasing Lifetimes in Diamond Using Transient Coherent Ultrafast Phonon Spectroscopy. *Diamond Relat. Mater.* **2010**, *19*, 1289−1295.
(60) Perdew, J. P.; Burke, K.; Ernzerhof, M. Generalized Gradient Approximation Made Simple. *Phys. Rev. Lett.* **1996**, *77*, 3865−3868.
(61) Baroni, S.; de Gironcoli, S.; Dal Corso, A.; Giannozzi, P. Phonons and Related Crystal Properties from Density-Functional Perturbation Theory. *Rev. Mod. Phys.* **2001**, *73*, 515−562.

https://doi.org/10.1021/acsami.2c10879
ACS Appl. Mater. Interfaces XXXX, XXX, XXX−XXX